Current Opinion in Colloid & Interface Science 20 (2015) 244–252

Contents lists available at ScienceDirect

Current Opinion in Colloid & Interface Science

journal homepage: www.elsevier.com/locate/cocis

Structural characterization of soft interfaces by standing-wave fluorescence with X-rays and neutrons

Emanuel Schneck [a,*], Bruno Demé [b]

[a] Biomaterials Department, Max Planck Institute of Colloids and Interfaces, Am Mühlenberg 1, 14476 Potsdam, Germany
[b] Institut Laue-Langevin, 71 avenue des Martyrs, 38042 Grenoble Cedex 9, France

ARTICLE INFO

Article history:
Received 24 June 2015
Received in revised form 26 June 2015
Accepted 27 June 2015
Available online 3 July 2015

Keywords:
Biological interfaces
Element profiles
X-ray and neutron scattering
Ions at interfaces

ABSTRACT

We present a review of standing-wave fluorescence techniques with x-rays and neutrons for the element-specific structural investigation of interfaces. The basic principles are introduced and typical measurement configurations with their advantages and limitations are compared. An overview of studies dealing with various types of interfaces is given. In particular, work on soft and biological matter in planar, interfacial geometries is discussed.

1. Introduction

The characteristics of soft matter in the vicinity of interfaces govern a multitude of phenomena in biology, technology, and biotechnology. The architecture of functional biomolecular assemblies, the texture foams, or the performance of biocompatible surfaces depend on the way molecules and ions self-organize near the "soft" interfaces between a liquid phase on one side and a solid, a liquid, or a gas phase on the other side [1,2]. Key components of biological matter often exhibit interfacial geometries. Biomembranes, for instance, can be viewed as two-dimensional molecular architectures mainly composed of lipids and proteins in an aqueous environment [3,4]. In order to understand the diversity of phenomena at soft interfaces, well defined model systems with planar geometries have been established, including molecular monolayers at liquid/gas [5] and liquid/liquid [6] interfaces as well as molecular mono- [7], bi- [8], and multilayers [9] on planar solid supports, among others. They have been investigated in various aspects including structure [10,11], mechanics [9,12,13], and dynamics [14]. Processes at soft interfaces typically involve the spatial reorganization of molecules, changes in molecular conformations, or the adsorption of ions or molecules in a chemically heterogeneous environment [15,16]. Structural insight on the nanometer scale is therefore a prerequisite to understand the complex behavior of molecular assemblies and the associated molecular interactions.

X-ray and neutron scattering are powerful tools to study the structure of interfaces at molecular length scales [17,18]. In contrast to other surface probes with high spatial resolution, such as atomic force or electron microscopy, they can access "buried interfaces", are usually non-destructive, and can be used under a wide range of conditions including ambient and physiological conditions. Scattering techniques have substantially contributed to our understanding of the structure of soft interfaces. They become especially powerful when samples possess planar geometry, allowing the specific probing of structures perpendicular and parallel to the surface. While grazing-incidence small-angle scattering yields information on the in-plane structure of an interface [11], reflectometry reveals matter density profiles perpendicular to the interface [18]. However it is generally difficult to elucidate molecular conformations and elemental distributions from such "global" density profiles. In contrast, standing-wave fluorescence techniques are suited to determine element-specific density profiles across an interface at sub-nm resolution.

Standing waves (SW) are generated wherever the interference of coherent waves occurs. Significant spatial intensity variations in the SW emerge when the intensity of two waves is of comparable magnitude. In the 1960s, Batterman and coworkers demonstrated that the interference of partial x-ray waves coherently diffracted from the lattice of a crystal can give rise to an x-ray standing wave (XSW) inside the crystal [19]. The XSW exhibits periodic nodes and antinodes (minima and maxima) which are located in defined spatial relations to the atoms of the crystal lattice. The positions of nodes and antinodes depend on the angle of incidence of the x-ray beam with respect to the crystal orientation. Element-characteristic fluorescence is induced by the XSW via photoelectric ionization. Close to a Bragg condition the nodes and antinodes are most pronounced and therefore give rise to enhancement or reduction of the fluorescence from the various elemental

* Corresponding author. Tel.: +49 331567-9404; fax: +49 331567 9402.
E-mail address: schneck@mpikg.mpg.de (E. Schneck).

http://dx.doi.org/10.1016/j.cocis.2015.06.001
1359-0294/

species in the crystal [20]. As a result, the precise position of the elements in the crystal lattice is encoded in the dependence of the fluorescence intensity on the incident angle around the Bragg condition and can be reconstructed. At the beginning, this method was mainly used for the investigation of bulk crystalline materials, for instance in order to localize foreign atoms in the lattice [21]. Later, XSW fluorescence was also used to determine the precise positions of adsorbed atoms at crystal surfaces [22,23]. Application and theory of XSW fluorescence measurements with crystalline materials are described in detail in a review by Zegenhagen [24].

Neutron standing waves (NSW) were first identified indirectly, from "anomalous" neutron absorption [25,26]. Namely, absorption is enhanced when the antinodes of a standing neutron wave in a crystal overlap with neutron-capturing nuclides. Only much later, Zhang et al. [27] measured the characteristic fluorescence of ^{157}Gd purposefully induced by NSW.

Since these early demonstrations, SW fluorescence with x-rays and neutrons has gradually been further developed and has become applicable for the investigation of non-crystalline soft-matter systems and interfaces. When dealing with soft interfaces, studies typically investigate the nanometric distribution of elements perpendicular to the interface. In this case, the atomic structure of the matter and its influence on the reflection of x-rays and neutrons can usually be neglected. In this article we review SW fluorescence techniques with x-rays and neutrons for the structural investigation of surfaces with a focus on various types of soft interfaces.

2. Standing-wave fluorescence at interfaces

In a SW fluorescence experiment at an interface and irrespective of the type of incident radiation, the characteristic fluorescence of the species j of interest is recorded as a function of the angle of incidence θ at which the beam impinges onto the interface. Here, *species* may denote either an element or a nuclide. X-rays induce characteristic fluorescence via photoelectric ionization of chemical elements. The energy of the incident beam is typically at the order of 10^4 eV and must exceed the relevant absorption edge of the chemical element of interest. Neutrons induce characteristic fluorescence via neutron capture by certain nuclides and subsequent relaxation processes involving the emission of particles and photons in the hard x-ray or γ range [28]. In a SW fluorescence experiment, the angle-dependent fluorescence intensity from species j, $I_j(\theta)$, then encodes the density profile along the z direction (or "depth profile") $\rho_j(z)$ of that species near an interface. Namely, $I_j(\theta)$ is proportional to the spatial integral over the product of $\rho_j(z)$ and the known angle-dependent standing wave intensity $\Phi(\theta, z)$:

$$I_j(\theta) = B \int_{-\infty}^{\infty} \Phi(\theta, z)\rho_j(z)A_j(z)dz. \tag{1}$$

With that, Eq. (1) allows reconstructing the density profile of a species from the angle-dependent characteristic fluorescence of that species. For a given incident angle θ, $\Phi(\theta, z)$ follows from the interfacial scattering length density (SLD) profile and can be computed from a suitable slab model representation of the SLD via the phase-correct summation of all reflected and transmitted partial waves [29] as has been described previously [30,31]. $A_j(z)$ in Eq. (1) denotes the depth-dependent transmission of the emitted fluorescence of species j. It accounts for the fact that the fluorescence from regions buried more deeply in the layers is attenuated more strongly on its way to the detector [32]. In many cases, however, for instance when the target elements are confined in nanometric layers, the depth dependence of the attenuation can be safely neglected ($A_j \approx$ const). B is a pre-factor determined by the fluorescence yield of species j, the detection efficiency, and geometrical factors, and in general also depends on the incident angle [33].

As implied in the introduction, SW fluorescence experiments generally require standing waves with pronounced spatial intensity variations. This in turn requires that the intensity of the reflected wave is comparable to that of the incident wave. Fig. 1 schematically illustrates typical measurement configurations where strong reflections are exploited in order to generate strongly modulated standing waves in the vicinity of the planar interface of interest:

a) An interface between two homogeneous media (Fig. 1a). Total reflection from the interface is achieved when the interface is illuminated through the medium of lower SLD (medium 1) at an incident angle θ below the critical angle of total reflection θ_c for this configuration. As shown in the corresponding reflectivity curve (Fig. 1a bottom), the reflectivity drops rapidly for $\theta > \theta_c$. The total reflection below θ_c gives rise to a long-period SW in medium 1 (Fig. 1a top). Only the exponentially decaying evanescent tail of the SW reaches into medium 2. As θ is increased from zero to θ_c, the nodes and antinodes in medium 1 move towards the interface while the period becomes gradually smaller. At the same time the decay length of the evanescent wave in medium 2 increases until it diverges at θ_c [17]. The standing waves are schematically depicted exemplarily for incident angles far below and close to θ_c, as indicated in the corresponding reflectivity curve. It is seen that different regions in the vicinity of the interface are probed by the SW for the two angles.
b) Thin layers at the interface between two homogeneous media (Fig. 1b). The situation is qualitatively similar to the one in Fig. 1a, but the SW assumes slightly more complex shapes due to the contribution of additional partial waves present within the layers. Moreover, layers at the interface in general shift the positions of nodes and antinodes.
c) A homogeneous medium in contact with a periodically structured solid (Fig. 1c). Close to a Bragg condition of the periodic structures at θ_B, the beam is strongly reflected, as schematically depicted in the corresponding reflectivity curve (Fig. 1c bottom). The Bragg condition typically occurs at angles much higher than the critical angle of total reflection ($\theta_B >> \theta_c$), so that the SW formed in medium 1 is characterized by a shorter period (Fig. 1c top) which coincides with that of the periodic solid structure. As θ is increased through the strong reflection condition, the nodes and antinodes of the standing wave gradually move towards the interface by half a period and probe structures within one period with high spatial resolution.

An instructive description of the behavior of standing waves in total reflection and Bragg reflection conditions is given in [34].

3. Standing-wave fluorescence with x-rays

Since the first demonstration of fluorescence induced by x-ray standing waves in bulk crystalline materials by Batterman [20], the technique has been adapted also for planar geometries.

3.1. Solid surfaces

The first fluorescence measurements under conditions of total reflection of x-rays were carried out by Yoneda and Horiuchi [35]. Their measurement configuration corresponds to Fig. 1a, where medium 1 is air and medium 2 is a planar solid. Using the same configuration, Becker et al. [36] illuminated a planar Ge surface with x-rays around the critical angle of total reflection and measured the angle-dependent fluorescence of Ge. The results were compared to theoretical models in the spirit of Eq. (1) and remarkable agreement was achieved.

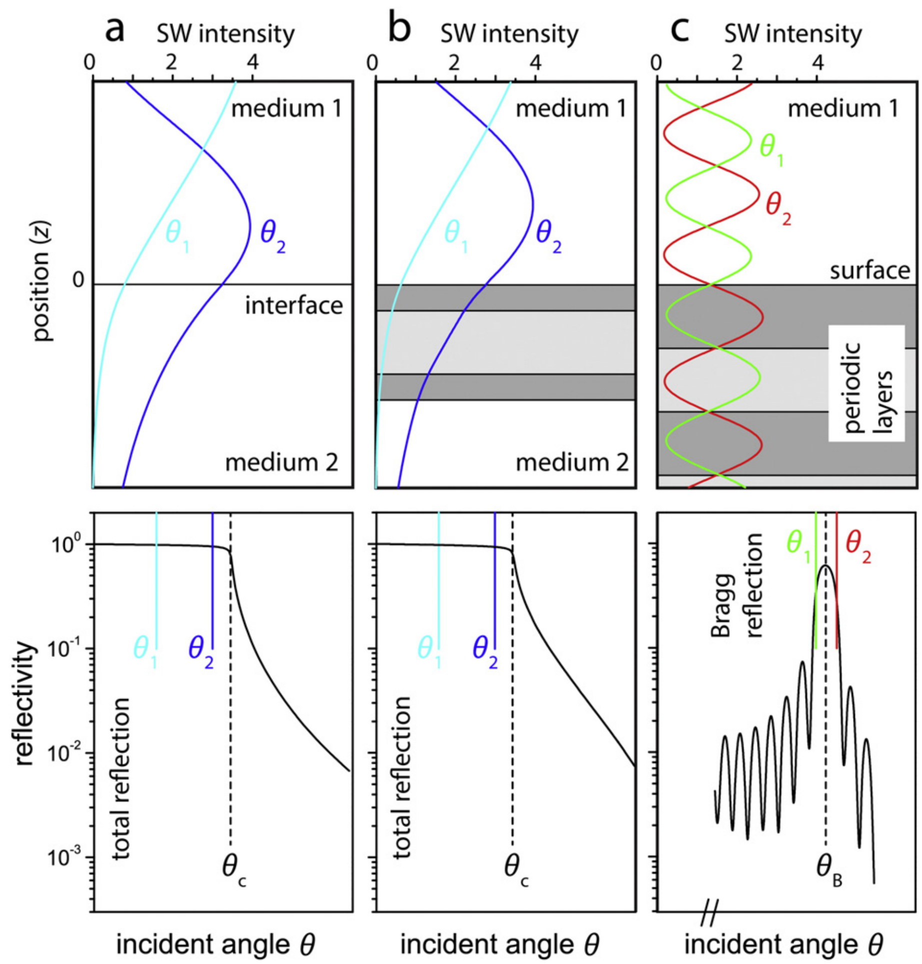

Fig. 1. Typical measurement configurations in SW fluorescence experiments. Schematic illustration of standing waves at an interface (top) for incident angles θ_1 and θ_2 indicated in the corresponding angle-dependent reflectivity curves (bottom). (a) Two homogeneous media illuminated far below (θ_1) and close to (θ_2) the critical angle for total reflection θ_c. (b) Thin layers at the interface between two homogeneous media illuminated at the same two angles. (c) A homogeneous medium in contact with a periodically structured solid illuminated for two angles slightly below (θ_1) and slightly above (θ_2) the Bragg angle θ_B.

3.1.1. Material on solid surfaces

In the aforementioned pioneering study by Yoneda and Horiuchi [35] traces of $NiCl_2$ salt were deposited on a glass surface. Due to the rapidly decaying evanescent tail of the SW in the glass (see Fig. 1a, medium 2), only a nanometer-thin region of the material is illuminated, so that undesired fluorescence background is dramatically reduced. As a consequence, Ni was detected from its characteristic fluorescence with unprecedented sensitivity. The sensitivity limit was predicted to be at the level of nanograms, which was later confirmed by Aiginger & Wobrauschek [37]. The same technique was later applied for the trace elemental analysis of solids [38] and impurities in liquids [39] with minimal sample amounts. The field of trace analysis using fluorescence under total x-ray reflection has been reviewed by von Bohlen [40] and by Klockenkämper [41].

3.1.2. Thin solid films on solid substrates

XSW fluorescence was used for the study of solid layered structures on top of solid substrates, corresponding to the configuration illustrated in Fig. 1b. Weisbrod et al. [32] determined density profiles of Si, Pd, Fe, Ni, and Cr in thin solid layers one of which was formed by an alloy of Ni, Fe, and Cr. Barbee and Warburton [42] deposited a sub-nanometer thin layer of Hf on top of a Pt/C multilayer with $\approx$ 3 nm periodicity. They measured and modeled the angle-dependent Hf and Pt fluorescence in total reflection but also in Bragg reflection. The latter corresponds to the configuration illustrated in Fig. 1c, when medium 1 is air and the thin Hf layer is located right at the interface between the periodic structure and medium 1. In that study, for the first time a synthetic structure with a purposefully chosen periodicity was designed to generate an XSW with a period of few nanometers. An overview on XSW fluorescence studies on thin solid films is given in a review article by Stoev and Sakurai [43].

3.1.3. Thin organic films on top of solid surfaces

Nakagiri et al. [44] deposited surfactant multi-bilayers on a planar solid support. The periodic internal structure of this organic film was exploited to generate a Bragg reflection that led to the formation of an XSW at the interface and within the multi-bilayers. Compare Fig. 1c when medium 1 is air and the periodic layers represent the organic film with periodic internal structure. The surfactant headgroup regions were selectively loaded with Pb or Mn, of which the fluorescence was induced with the angle-dependent XSW. In this way, the positions of Pb and Mn were determined from their angle-dependent characteristic fluorescence. Bedzyk et al. [34] used XSW fluorescence to study the structure of an organic film on top of a substrate with periodic W/Si multilayers. The film was formed by three surfactant monolayers, selectively loaded in the headgroup region with Zn or Cd. The distributions of these heavy atoms, characterized by their center positions and their widths, were determined with a resolution of a few angstroms as a function of the temperature. Fig. 2 shows the angle-dependent reflectivity (bottom curve) and the Zn K_α fluorescence intensities for various temperatures. Solid lines are the best-matching theoretical curves

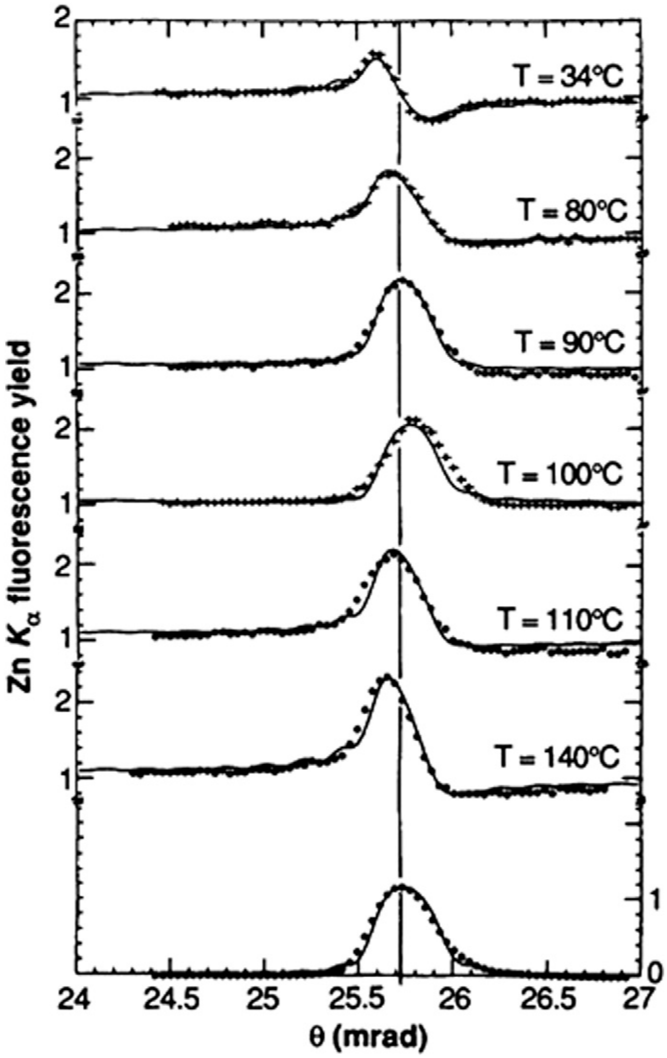

Fig. 2. Angle-dependent reflectivity around the Bragg condition (bottom curve) and Zn K_α fluorescence intensities from Zn-labeled surfactant oligo-layers on top of a substrate with periodic W/Si multilayers for various temperatures. Solid lines are the best-matching theoretical curves corresponding to different positions and widths of the Zn distribution. From [34].

corresponding to different positions and widths of the Zn distribution. In addition to the Bragg reflection configuration (Fig. 1 c, when the organic layer sits on top of the periodic structure), which yielded the high spatial resolution, also the total reflection configuration, which probes a larger spatial range, was realized in order to obtain unambiguous results. In a subsequent study by the same group, the distribution of Zn confined at about 20 nm from the reflecting surface in a surfactant multilayer architecture was determined with remarkably high spatial resolution [45], demonstrating the great potential of long-period XSW as generated in a total reflection configuration. Later, heavy atoms were localized in the same way in even larger organic architectures and larger distances from the reflecting surface [46] and the influence of the roughness of the reflecting surface on the effective width of elemental distributions was discussed [47]. Similar approaches were used by another group to study Mn and Pb loaded stearic acid in multilayers on solid substrates [48] and Pb atoms in thin protein/lipid films deposited on solid substrates before and after treatment with a Pb-chelating agent [49]. More recently, ion distributions in polyelectrolyte multilayers were studied [50]. Br^- ions were localized in alternating polyelectrolyte layers of positive and negative charge after emersion from an aqueous electrolyte. The amount of remaining Br^- ions as well as their distribution was found to be strongly influenced by the charge sign of the terminal layer and thus by the effective charge of the surface.

3.2. Solid/liquid interfaces

The first study of solid/liquid interfaces using XSW fluorescence was carried out by Cowan et al. [22]. A short-period XSW was generated by Bragg reflection from the diffraction planes of an oriented silicon crystal. This configuration corresponds to Fig. 1c, when medium 1 is the liquid phase, and the periodic solid structure represents the diffraction planes of the silicon crystal. Bromine atoms, covalently adsorbed onto the silicon surface from a methanol solution were spatially localized with crystallographic resolution from their angle-dependent characteristic fluorescence. In order for such a measurement to be sensitive to the interfacial element distribution, the amount of the element of interest at the interface must be at least comparable to the total amount of this element in the bulk liquid. In addition, absorption of the incident and fluorescence radiation in the liquid can constitute a significant experimental challenge that is typically approached by the use of microfluidic or nanofluidic chambers. Bedzyk and coworkers performed the first fluorescence study on a solid/liquid interface with a long-period XSW [51]. Ion distributions near a charged solid-supported model membrane surface were determined from fluorescence measurements around the total reflection region. This configuration is best illustrated in Fig. 1 b, when medium 1 is the aqueous phase, medium 2 is the planar solid and the layers at the interface between the two media represent the supported model membrane. In that study, a substantial decrease in the extension of the diffuse ionic double layer with increasing ionic strength was observed, in qualitative agreement with the Gouy–Chapman model. Later on, distributions of Rb^+ and Sr^+ ions at a negatively-charged titanium oxide surface were probed with short-period standing waves [52]. The experiments enabled determining the partitioning of ions between the condensed and diffuse parts of the electric double layer. More recently, the end segment distribution of a polymer brush grafted to a solid surface was investigated [53]. Each end segment was covalently labeled with a Ge atom, of which the fluorescence was induced by an XSW under total reflection. End segment distributions were measured for the dry surface in air, where the end segments were found to be confined in a thin plane at a certain distance from the grafting surface (i.e., the reflecting surface). For the surfaces in contact with a good solvent for the polymers, a broad distribution was observed.

3.3. Liquid/gas interfaces

The first XSW fluorescence study at a liquid/gas interface by Bloch et al. dealt with the distribution of Mn-labeled polymers near the interface between air and liquid DMSO [54]. The measurement configuration corresponds to Fig. 1a, when medium 1 is air and medium 2 is the liquid. It is worth noting that at the liquid/gas interface the liquid is the medium with higher electron density and thus higher SLD for x-rays, which is in contrast to the typical situation for solid/liquid interfaces. As a consequence, the liquid medium is probed with the exponentially decaying evanescent tail of the XSW under total reflection at the liquid/gas interface. This, in turn, means that undesired background fluorescence from the bulk liquid medium is suppressed, so that the interfacial distribution of chemical elements can be probed with high sensitivity, albeit with the inherently poorer spatial resolution associated with the evanescent wave. The methodology of XSW fluorescence under total reflection and its application to liquid/gas interfaces is explained in more detail in [31].

3.3.1. Ions at charged monolayers

In another study by Bloch et al., the excess of Mn^{2+} ions at a negatively charged stearic acid monolayer immobilized at an air/water interface was quantified [55]. The absolute number of Mn^{2+} ions per stearic acid molecule was worked out from the Mn fluorescence of the bulk solution with known $MnCl_2$ concentration and from the known area per stearic acid molecule. Using the same strategy, Daillant et al. determined excesses of counter- and co-ions at charged lipid monolayer as a function of monolayer lateral density and found a constant counter-ion to lipid ratio throughout the isotherm [56]. It should be mentioned that thin organic layers at an air/water interface, such as a surfactant monolayer, significantly influence the SLD profile across the interface and thus the shape of the XSW. This is in contrast to thin organic layers on the surface of a solid, where the electron density gradient is typically dominated by the surface of the dense solid medium, so that the thin organic layers only weakly affect the XSW. Later on, XSW fluorescence was employed by Antipina et al. to determine the protonation state of cationic lipids in monolayers at the air/water interface by quantification of the counter ion excess (Br^-) as a function of pH and lipid lateral density [57]. In another study by the same group, the competitive adsorption excess of various monovalent and divalent cations to negatively charged behenylsulfate monolayers was determined and pronounced ion specificity was observed and interpreted in terms of different hydrated ion sizes [58]. Small monovalent cations were found to be able to compete with large divalent cations under certain conditions. More recently, excesses and approximate distributions of monovalent and divalent cations at comparatively realistic, negatively charged models of bacteria surfaces were determined in the absence and presence of cationic antimicrobial peptides [30,59]. Fig. 3 shows angle-dependent K K_α fluorescence intensities from a monolayer of mutant lipopolysaccharides (LPS Re, see inset) at an air/water interface on 100 mM KCl. Shown are relative intensities, after division by the intensities obtained at the same angles with the bare aqueous phase, i.e., in the absence of the monolayer. The solid line indicates the best-matching model, in which a narrow K^+ distribution with a maximum at $z_{\max} = 5$ Å from the interface between hydrophobic alkyl chains and hydrated saccharide headgroups is assumed. The agreement between experimental data and the model is very good. As indicated with the dashed line, the agreement is significantly worse when a broader distribution peaking at $z_{\max} = 20$ Å is assumed.

3.3.2. Organic adsorbates and internal structure of organic layers

The amount of Br-labeled DNA adsorbed per unit area to a positively charged lipid monolayer was quantified by measurements of the characteristic fluorescence of Br under x-ray total reflection [60]. It was shown that the adsorption affinity of (multi-anionic) DNA to the surface is much stronger than that of anions, and, in contrast to the naïve expectation, increases with the solution's ionic strength. Approximate positions of heavy elements in surfactant and lipid monolayers at air/water interfaces were measured from their angle-dependent characteristic fluorescence around the critical angle of total reflection [61]. More recently, excesses and approximate depth profiles of complexed Ni^{2+} ions and chemically bound S atoms in a bio-mimetic model system involving a complicated architecture of lipid and protein layers were determined [62].

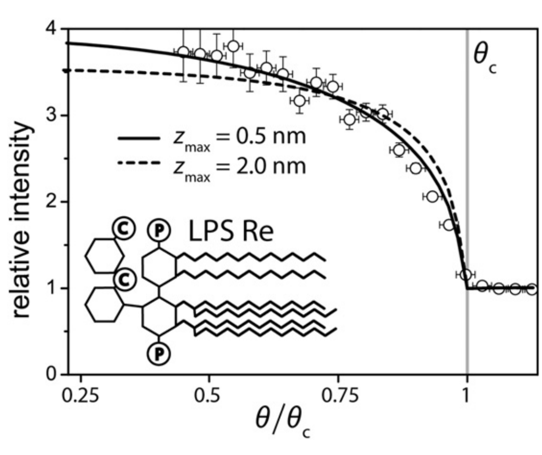

Fig. 3. Angle-dependent K K_α fluorescence intensities from a monolayer of LPS Re at an air/water interface on 100 mM KCl. Shown are relative intensities, after division by the intensities obtained with the bare aqueous phase. Lines are theoretical intensities that correspond to different models of the interfacial K^+ distribution, assuming the maximum at $z_{\max} = 5$ Å (solid line) and $z_{\max} = 20$ Å (dashed line) from the interface between hydrophobic alkyl chains and hydrated saccharide headgroups. The inset illustrates the chemical structure of LPS Re, where C and P denote negatively charged carboxyl and phosphate groups, respectively. Adapted from [30].

3.3.3. Ions at the bare air/water interface

Padmanabhan et al. studied ion interactions with the bare air/water interface [63]. The long-debated weak depletion of ions at the air/water interface on concentrated salt solutions was quantified with high accuracy. Fig. 4 shows angle-dependent, normalized K^+ and Cl^- fluorescence intensities from the surface of a 100 mM KCl solution. Lines are modeled intensities corresponding to image charge interactions with the air/water interface only (dashed line) and for an additional ion-free layer of thickness $d = 0.377$ nm (solid line). The obtained depletion layer, resulting from non-Coulombic interaction contributions is in line with the well known Hofmeister effect.

3.4. Liquid/liquid interfaces

XSW fluorescence work on liquid/liquid interfaces is still sparse, mainly because of the experimental challenges associated with liquid/liquid interfaces in general, for instance interfacial curvature induced by menisci. In addition, the attenuation of incident and fluorescence radiation by the liquid media and the requirement of horizontal sample geometries pose limitations to the fluorescence detection efficiency. Only recently, Bu et al. reported the quantification by XSW fluorescence under total reflection of heavy ion amounts immobilized at oil/water interfaces via extractant molecules [64,65]. Their measurement configuration corresponds to Fig. 1a when medium 1 is the oil phase and medium 2 the aqueous phase.

3.5. Light elements at soft interfaces

Most XSW fluorescence work on soft interfaces has so far dealt with the fluorescence of comparatively heavy elements, which facilitates the experiments due to their high fluorescence yields. Even models of biological surfaces have typically been labeled, in one way or another, with heavy elements that are not naturally abundant in biological matter. In contrast, comparatively light elements like P and S are found ubiquitously in all main classes of biomolecules covalently bound at well-known position in the chemical structures. P and S, but also the light but biologically relevant ions Na^+ and Mg^{2+} are, thus, highly interesting targets for XSW fluorescence studies. However, only

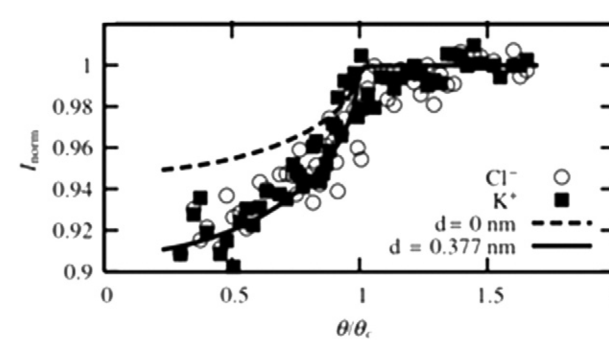

Fig. 4. Angle-dependent, normalized K^+ and Cl^- K_α fluorescence intensities from the surface of a 100 mM KCl solution. Lines are modeled intensities corresponding to image charge interactions with the air/water interface only (dashed line) and for an additional ion-free layer (solid line). From [63].

a handful of studies report on the localization of such light elements by XSW fluorescence [62,66,67]. For example, Zheludeva et al. determined the distribution of phosphorus in a relatively thick (>100 nm) protein/phospholipid film at an air/water interface [67]. All these studies dealt with either gas/liquid or gas/solid interfaces, where limitations due to the adsorption of low-energy incident and fluorescence radiation as well as undesired background fluorescence are largely circumvented. Future studies on light elements at solid/liquid or liquid/liquid interfaces will have to tackle these challenges.

4. Standing wave fluorescence with neutrons

Fluorescence induced by neutron standing waves (NSW) is based on the emission of radiation after neutron capture and is applicable to systems containing nuclides with high cross sections for neutron capture—such as ^{157}Gd, ^{149}Sm, ^{113}Cd, ^{10}B, and ^{6}Li—(see Table 1), or where they can be used as labels. Not all strong neutron capturers are heavy elements. Boron (B), for instance, is light and more generally applicable as a label from a chemical viewpoint, as it is accessible to covalent chemistry.

4.1. Thin films on solid surfaces

The first NSW fluorescence experiments performed at NIST in the 1990s by Zhang et al. [27] exploited the phenomenon of prompt γ emission (PGE) after neutron-capture. In this study the authors report on simultaneous measurements of the characteristic γ fluorescence at 182 keV from the ^{157}Gd(n, γ)^{158}Gd reaction and neutron reflectivity on a solid-supported polymer film with an embedded 5 nm thick Gd_2O_3 layer (see inset Fig. 5a for a sketch). The measurement configuration corresponds to the one illustrated in Fig. 1b, when medium 1 is air and medium 2 the solid support. Below the critical angle of total reflection, enhanced γ fluorescence was observed for incident angles that also exhibited pronounced minima in neutron reflectivity (Fig. 5a and b). These minima correspond to reflection conditions where the neutron standing waves are resonantly amplified in the film and thus most strongly absorbed by the Gd_2O_3 layer. By simultaneously fitting γ-fluorescence intensity and reflectivity data the authors were able to characterize the depth profile of the polymer film and to localize the Gd_2O_3 layer. The sensitivity of the combination of fluorescence and reflectivity data to the buried Gd_2O_3 layer and its depth profile was demonstrated to surpass that of neutron reflectivity analysis alone.

NSW fluorescence experiments on solid-supported layered films were also performed by Aksenov and coworkers. In a study on a layered magnetic Fe/Gd structure deposited on a glass substrate, two polarization states of a neutron beam were used. The difference between the NSW formed with the two polarization states was quantified via the characteristic γ fluorescence after neutron capture by Gd [69]. In another study [70], neutron resonance in a ^{6}LiF/Ti/Cu/glass layered structure was quantified in simultaneous measurements of neutron reflectivity and the ^{6}Li(n, α)^{3}H nuclear reaction as fluorescence signal. The observation of the neutron density resonant character in the Ti spacer needed a neutron absorbing layer which was the ^{6}LiF cap layer itself. Similarly to the work of Zhang et al. [27], minima in the reflectivity curve correspond to maxima in the α and ^{3}H emission, i.e., the fluorescence intensity. This intensity maximum reflects the amplification of the NSW in the ^{6}LiF cap layer as it results from the resonance condition in the spacer layer. In another study by Aksenov and co-workers it was shown that experiments with NSW can yield specific structural information without the use of element-specific fluorescence radiation [71]. A NSW with a particular spin state was generated in a Cu/Ti/Co/Ti multilayer structure on a glass substrate in a magnetic field. The standing wave was used to localize with high spatial resolution a “spin flipper layer” that causes changes in the neutron spin. An overview of NSW fluorescence experiments on solid-supported thin layers and the theory for data interpretation is given in [72], and the technique is further reviewed in [73].

Table 1
Thermal neutron capture cross sections σ of various nuclides for neutrons with a velocity of $v = 2200$ m/s [68], corresponding to a wavelength of $\lambda = 1.8$ Å. Note that σ exhibits strong λ-dependence and is significantly higher for measurements with cold neutrons. For example, $\sigma(^{157}\mathrm{Gd}) = 580{,}000$ Barns at $\lambda = 5$ Å.

Nuclide	Natural abundance (%)	Absorption cross section σ (Barns)
^{157}Gd	16	254,000
^{149}Sm	14	40,100
^{113}Cd	12	20,600
^{10}B	20	3840
^{6}Li	7.5	940

4.2. Solid/liquid interfaces

More recently, NSW fluorescence was used by Schneck et al. for the study of a lipid membrane at a planar solid/water interface [33]. The architecture of the sample is illustrated in the inset of Fig. 6a. The membrane was labeled with $^{157}Gd^{3+}$ ions bound from a dilute aqueous $GdCl_3$ solution to chelator motifs at the membrane surface at a lateral density as low as one Gd atom per nm^2. The Gd amount in this submonolayer was more than two orders of magnitude lower than in the in the Gd or Gd_2O_3 layers investigated in previous studies, so that an unprecedented sensitivity for the characteristic fluorescence at 182 keV from the Gd labels was required. Strict surface sensitivity was achieved by illumination of the solid/liquid interface with the neutron beam entering through the solid medium, a silicon crystal. This measurement configuration corresponds to the one illustrated in Fig. 1b, when medium 1 is silicon and medium 2 the aqueous phase. The latter is probed only with the exponentially decaying evanescent tail of the NSW under total reflection conditions, i.e., for $\theta < \theta_c$, so that fluorescence background from Gd in the bulk aqueous medium is suppressed. A condition of total reflection of the neutron beam from the aqueous phase at the solid/water interface is conveniently realized when heavy water (D_2O) with a high SLD, is used instead of normal light water (H_2O). This is in contrast to the case of x-rays, because the electron density of water is lower than that of commonly used solids. In order to further improve the sensitivity additional measures were taken: Under-illumination of the interface at all incident angles was ensured through a narrow neutron beam collimation. Moreover, great care was taken to shield the γ-detector from background radiation. The main panel of Fig. 6a shows angle-dependent intensities of the neutron-induced fluorescence of ^{157}Gd from the labeled membrane surface illustrated in the figure inset. The lines superimposed on the data points represent theoretical predictions of the angle-dependent fluorescence intensities for various positions z_0 of the ^{157}Gd labels with respect to the membrane surface. Only solid black and dashed red lines, corresponding to $z_0 = 0.5$ nm and $z_0 = 1$ nm, respectively, are in agreement with the measured data points within the error, while the other two scenarios can be excluded. These results demonstrated that NSW fluorescence has the potential to localize labeled molecules at solid/liquid interfaces with nanometer precision. In the same study [33] the label density was probed down to lower surface densities by reducing the complexation efficiency between Gd^{3+} and the chelator motifs. The result was in good qualitative agreement with titration curves of the chelator–lanthanide complexes.

In a very recent experiment the method was extended to labeled proteins [74]. The protein neutravidin (NA, from Life Technologies, Darmstadt, Germany), a deglycosylated version of streptavidin (SA), was labeled with ^{157}Gd using the commercially-available labeling tool PROTrack^{TM} (BioPAL Inc., Worcester MA, USA) and then bound from a dilute aqueous $GdCl_3$ solution (5 μM $GdCl_3$, 2.5 mg/mL NA, 100 mM NaCl, 5 mM MES, pH 6) to a solid-supported lipid bilayer (SOPC) containing 5 mol% biotinylated lipid (DOPE-cap-biotinyl, Avanti Polar Lipids, Alabaster AL, USA). The biotin–SA complex is known for its

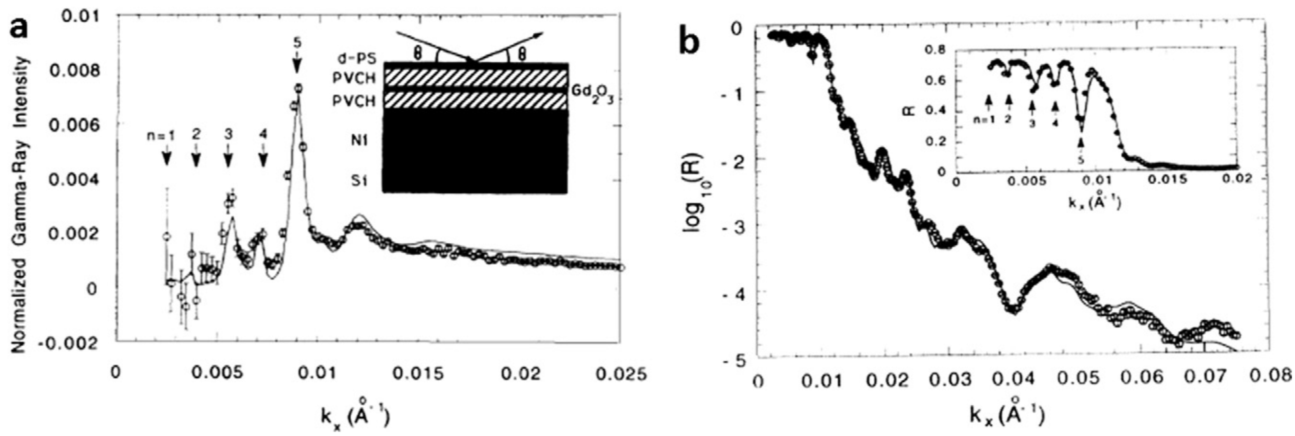

Fig. 5. (a) Characteristic γ fluorescence of ^{157}Gd after neutron capture, measured from a layered magnetic Fe/Gd structure as a function of the incident angle, which is expressed in terms of the normal component of the incident wave vector, $k_x = (2\pi/\lambda)\sin\theta$. Here, λ denotes the neutron wavelength. Inset: Illustration of the sample structure. (b) Intensity of the neutron beam reflected from the same structure as a function of k_x. The solid line in both panels is a theoretical curve corresponding to the best-matching common model. From [27].

strong affinity and stability. The sample architecture is illustrated in the inset of Fig. 6b. In this study performed on D16 at the ILL (Grenoble, France), the instrument setup and the methods were the same as described in [33]. The main panel of Fig. 6b shows angle-dependent intensities of the neutron-induced fluorescence of ^{157}Gd from the labeled NA proteins as illustrated in the figure inset. The line superimposed on the data points represents a model prediction of the fluorescence intensities for a broad distribution (fwhm: 2.5 nm) of ^{157}Gd centered 2 nm above the surface of the supported lipid bilayer. This plausible scenario is in agreement with the data points. However, the statistics of the experimental data were insufficient for a precise determination of the label distribution. In fact, the low absolute intensity of the characteristic γ-fluorescence suggested that the protein was rather poorly labeled with ^{157}Gd, at the order of one Gd atom per protein, corresponding to the order of one Gd atom per 10 nm^2. It should be noted that in all these NSW fluorescence experiments at the solid/liquid interface a monochromatic cold neutron beam was used. The use of the recently upgraded D16 instrument at the ILL (×10 flux gain at the sample) or time-of-flight neutron reflectometers with much higher neutron flux could further improve the sensitivity by an order of magnitude.

4.3. Liquid/liquid interfaces

An interesting application for NSW fluorescence in the future may be the element-specific structural investigation of liquid/liquid interfaces. At first, a high contrast in neutron SLD can be achieved at the interface between the two liquids via selective deuteration, which is in contrast to the case of x-rays, where typical liquids tend to have similar electron densities and thus x-ray SLDs. Secondly, many liquids have low absorption coefficients for neutrons, so that the liquid/liquid interface is conveniently accessible. Finally, the high energy fluorescence photons induced by the NSW can easily penetrate through thick liquid layers and thus be effectively detected. With that, NSW fluorescence may be a powerful technique in the field of separative chemistry, in particular for the extraction of lanthanides, such as Gd, at oil/water interfaces [75].

5. Concluding remarks

Over the last five decades SW fluorescence techniques with x-rays and neutrons have constantly evolved and become versatile tools for the element-specific structural characterization of various sorts of interfaces including “soft” interfaces with liquid media as well as

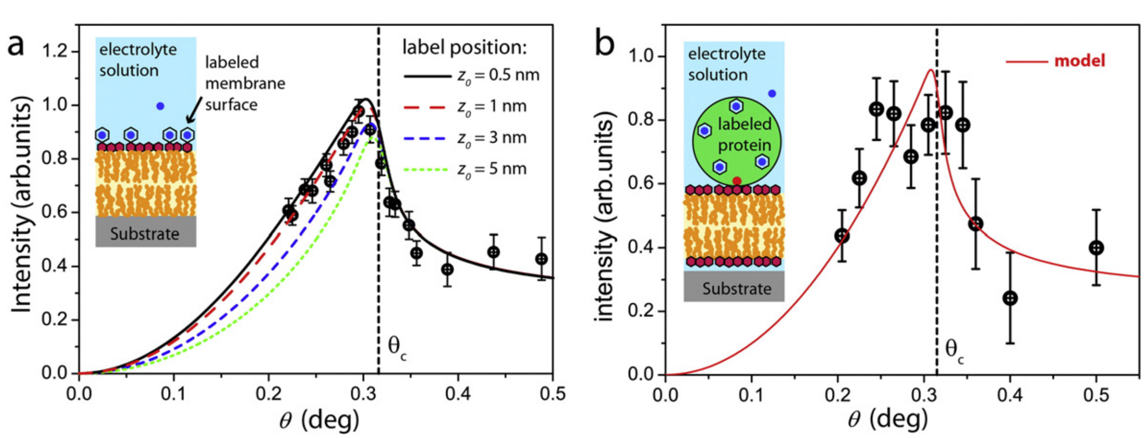

Fig. 6. (a) Inset: Schematic drawing of a ^{157}Gd-labeled membrane at the interface between an aqueous electrolyte and a silicon substrate. Main panel: Characteristic γ-fluorescence intensity from the labeled membrane surface as a function of the incident angle. Lines are model predictions for various positions z_0 of the ^{157}Gd labels with respect to the membrane surface. Adapted from [33]. (b) Inset: Schematic drawing of a ^{157}Gd-labeled protein layer bound onto a supported lipid bilayer. Main panel: Fluorescence intensity from the labeled proteins as a function of the incident angle. The line is a model prediction for a 2.5 nm broad ^{157}Gd distribution centered 2 nm above the surface of the supported bilayer [74].

biomolecular layers at planar interfaces. SW fluorescence can therefore be expected to find more common use also in soft-matter and biological sciences. The localization of several biologically relevant yet comparatively light elements is still challenging but technically feasible. With that, the label-free element-specific structural characterization of biological matter in planar interfacial geometries with near-crystallographic resolution is within reach. Such studies will reveal the structure of biomolecular systems with unprecedented detail and also allow for comprehensive comparison with atomistic computer simulations.

Acknowledgments

We thank Jean Daillant, Oleg Konovalov, Dmitri Novikov, Motomu Tanaka, and Gerald Brezesinski for discussions and insightful comments. The authors are gratefull to the ILL and ESRF for the allocations of beamtime and for technical support. We thank Michael Jentschel for his support in the γ detection for the NSW studies performed at ILL. E. S. acknowledges support by an Emmy-Noether grant (SCHN 1396/1) of the German Research Foundation (DFG) and by a Marie Curie Intra-European Fellowship (grant N. 299676) within the European Commission seventh Framework Program.

References•,••

[1] Adamson AW, Gast AP. Physical chemistry of surfaces; 1967.
[2] Evans DF, Wennerström H. The colloidal domain—where physics, chemistry, biology, and technology meet. Advances in interfacial engineering. New York: VCH; 1994.
[3] Lipowsky R, Sackmann E. Structure and dynamics of membranes: I. from cells to vesicles/II. generic and specific interactions. Elsevier; 1995.
[4] Mouritsen OG. Life—as a matter of fat. Springer; 2005.
[5] Möhwald H. Phospholipid monolayers. In: Lipowski R, Sackmann E, editors. Structure and dynamics of membranes. Amsterdam: Elsevier, E; 1995.
[6] Thoma M, Möhwald H. Phospholipid monolayers at hydrocarbon/water interfaces. J Colloid Interface Sci 1994;162(2):340–9.
[7] Schneck E, Papp-Szabo E, Quinn BE, Konovalov OV, Beveridge TJ, Pink DA, et al. Calcium ions induce collapse of charged O-side chains of lipopolysaccharides from *Pseudomonas aeruginosa*. J R Soc Interface 2009;6:S671.
[8] Sackmann E. Supported membranes: scientific and practical applications. Science 1996;271(5245):43–8.
[9] Salditt T. Thermal fluctuations and stability of solid-supported lipid membranes. J Phys Condens Matte 2005;17(6):R287–314.
[10] Kucerka N, Nagle JF, Sachs JN, Feller SE, Pencer J, Jackson A, et al. Lipid bilayer structure determined by the simultaneous analysis of neutron and X-ray scattering data. Biophys J 2008;95(5):2356–67.
[11] Als-Nielsen J, Jacquemain D, Kjaer K, Leveiller F, Lahav M, Leiserowitz L. Principles and applications of grazing incidence x-ray and neutron scattering from ordered molecular monolayers at the air–water interface. Phys Rep 1994;246(5):251–313.
[12] Daillant J, Bellet-Amalric E, Braslau A, Charitat T, Fragneto G, Graner F, et al. Structure and fluctuations of a single floating lipid bilayer. Proc Natl Acad Sci U S A 2005;102(33):11639–44.
[13] Schneck E, Demé B, Gege C, Tanaka M. Membrane adhesion via homophilic saccharide–saccharide interactions investigated by neutron scattering. Biophys J 2011; 100:2151.
[14] Trapp M, Gutberlet T, Juranyi F, Unruh T, Demé B, Tehei M, et al. Hydration dependent studies of highly aligned multilayer lipid membranes by neutron scattering. J Chem Phys 2010;133(16):164505.
[15] Israelachvili JN. Intermolecular and surface forces. 2 ed. London: Academic Press Inc.; 1991.
[16] Safran, S., Statistical Thermodynamics of Surfaces and interfaces. Vol. 103. 1994: Addison-Wesley, New York.
[17] Als-Nielsen J, McMorrow D. Elements of modern X-ray physics. Chichester: Wiley; 2001.
[18] Daillant J, Gibaud A. X-ray and neutron reflectivity: principles and applications. Berlin: Springer; 2009.
[19] Batterman BW, Cole H. Dynamical diffraction of X rays by perfect crystals. Rev Mod Phys 1964;36(3):681.
[20]•• Batterman BW. Effect of dynamical diffraction in X-ray fluorescence scattering. Phys Rev 1964;133(3A):A759. First XSW fluorescence measurements.
[21] Batterman BW. Detection of foreign atom sites by their X-ray fluorescence scattering. Phys Rev Lett 1969;22(14):703.
[22]• Cowan PL, Golovchenko JA, Robbins MF. X-ray standing waves at crystal surfaces. Phys Rev Lett 1980;44(25):1680. First XSW fluorescence measurements at solid/liquid interface. Localization of foreign atoms adsorbed to crystal surfaces.
[23] Golovchenko JA, Patel JR, Kaplan DR, Cowan PL, Bedzyk MJ. Solution to the surface registration problem using X-ray standing waves. Phys Rev Lett 1982;49(8):560.
[24] Zegenhagen Jr. Surface structure determination with X-ray standing waves. Surf Sci Rep 1993;18(7):202–71.
[25] Sippel D, Kleinstück K, Schulze GER. Nachweis der anomalen absorption thermischer neutronen bei interferenz am idealkristall. Phys Status Solidi B 1962; 2(5):K104–5.
[26] Knowles JW. Anomalous absorption of slow neutrons and X-rays in nearly perfect single crystals. Acta Crystallogr 1956;9(1):61–9.
[27]•• Zhang H, Gallagher PD, Satija SK, Lindstrom RM, Paul RL, Russell TP, et al. Grazing incidence prompt gamma emissions and resonance-enhanced neutron standing waves in a thin film. Phys Rev Lett 1994;72:3044–7. First NSW fluorescence measurements.
[28] ENSDF. Evaluated nuclear structure data file. www.nndc.bnl.gov/ensdf.
[29] Born M, Wolf E. Principles of optics. Cambridge university press; 1999.
[30]• Schneck E, Schubert T, Konovalov OV, Quinn BE, Gutsmann T, Brandenburg K, et al. Quantitative determination of ion distributions in bacterial lipopolysaccharide membranes by grazing-incidence X-ray fluorescence. Proc Natl Acad Sci U S A 2010;107:9147–51. Quantification and approximate localization of ions at realistic model of bacterial surface.
[31] Yun WB, Bloch JM. X-ray near total external fluorescence method: experiment and analysis. J Appl Phys 1990;68(4):1421–8.
[32] Weisbrod U, Gutschke R, Knoth J, Schwenke H. Total reflection X-ray fluorescence spectrometry for quantitative surface and layer analysis. Appl Phys A 1991;53(5): 449–56.
[33]•• Schneck E, Jentschel M, Gege C, Tanaka M, Demé B. Grazing-incidence neutron-induced fluorescence probes density profiles of labeled molecules at solid/liquid interfaces. Langmuir 2013;29(12):4084–91. First NSW fluorescence at solid/liquid interface.
[34]•• Bedzyk MJ, Bilderback DH, Bommarito GM, Caffrey M, Schildkraut JS. X-ray standing waves: a molecular yardstick for biological membranes. Science 1988; 241(4874):1788–91. Precise determination of heavy element distribution in surfactant oligo-layers.
[35]• Yoneda Y, Horiuchi T. Optical flats for use in X-ray spectrochemical microanalysis. Rev Sci Instrum 1971;42(7):1069–70. First use of total reflection x-ray fluorescence for elemental trace analysis.
[36] Becker RS, Golovchenko JA, Patel JR. X-ray evanescent-wave absorption and emission. Phys Rev Lett 1983;50(3):153.
[37] Aiginger H, Wobrauschek P. A method for quantitative X-ray fluorescence analysis in the nanogram region. Nucl Inst Methods 1974;114(1):157–8.
[38] von Bohlen A, Eller R, Klockenkaemper R, Toelg G. Microanalysis of solid samples by total-reflection X-ray fluorescence spectrometry. Anal Chem 1987;59(21):2551–5.
[39] Simabuco SM, Matsumoto E. Synchrotron radiation total reflection for rainwater analysis. Spectrochim Acta B At Spectrosc 2000;55(7):1173–9.
[40] von Bohlen A. Total reflection X-ray fluorescence and grazing incidence X-ray spectrometry tools for micro-and surface analysis. A review. Spectrochim Acta B At Spectrosc 2009;64(9):821–32.
[41] Klockenkämper R, Knoth J, Prange A, Schwenke H. Total-reflection X-ray fluorescence spectroscopy. Anal Chem 1992;64(23):1115A–23A.
[42] Barbee TW, Warburton WK. X-ray evanescent-and standing-wave fluorescence studies using a layered synthetic microstructure. Mater Lett 1984;3(1):17–23.
[43] Stoev KN, Sakurai K. Review on grazing incidence X-ray spectrometry and reflectometry. Spectrochim Acta B At Spectrosc 1999;54(1):41–82.
[44]• Nakagiri T, Sakai K, Iida A, Ishikawa T, Matsushita T. X-ray standing wave method applied to the structural study of Langmuir–Blodgett films. Thin Solid Films 1985; 133(1):219–25. XSW generated by periodic surfactant multilayers.
[45]• Bedzyk MJ, Bommarito GM, Schildkraut JS. X-ray standing waves at a reflecting mirror surface. Phys Rev Lett 1989;62(12):1376–9. Localization of heavy elements in thick organic multilayer architecture.
[46] Wang J, Bedzyk MJ, Penner TL, Caffrey M. Structural studies of membranes and surface layers up to 1,000 Ã… thick using X-ray standing waves. Nature 1991;354: 377–80.
[47] Zhang R, Itri R, Caffrey M. Membrane structure characterization using variable-period X-ray standing waves. Biophys J 1998;74(4):1924–36.
[48] Zheludeva SI, Kovalchuk MV, Novikova NN, Sosphenov AN, Erochin VE, Feigin LA. X-ray total external reflection fluorescence study of LB films on solid substrate. J Phys D Appl Phys 1993;26:A202–5.
[49] Novikova NN, Yurieva EA, Zheludeva SI, Kovalchuk MV, Stepina ND, Tolstikhina AL, et al. X-ray fluorescence methods for investigations of lipid/protein membrane models. J Synchrotron Radiat 2005;12:511–6.
[50] Schollmeyer H, Guenoun P, Daillant J, Novikov DV, von Klitzing R. Ion distribution in polyelectrolyte multilayers with standing-wave X-ray fluorescence. J Phys Chem B 2007;111:4036–42.
[51]•• Bedzyk MJ, Bommarito GM, Caffrey M, Penner TL. Diffuse-double layer at a membrane-aqueous interface measured with x-ray standing waves. Science 1990; 248(4951):52–6. Determination of ion distributions near a charged solid-supported model membrane surface.
[52] Fenter P, Cheng L, Rihs S, Machesky M, Bedzyk MJ, Sturchio NC. Electrical double-layer structure at the rutile–water interface as observed in situ with small-period X-ray standing waves. J Colloid Interface Sci 2000;225:154–65.
[53] Basu JK, Boulliard JC, Capelle B, Daillant J, Guenoun P, Mays JW, et al. Direct probe of end-segment distribution in tethered polymer chains. Macromolecules 2007;40: 6333–9.

• of special interest.
•• of outstanding interest.

[54] •• Bloch JM, Sansone M, Rondelez F, Peiffer DG, Pincus P, Kim MW, et al. Concentration profile of a dissolved polymer near the air–liquid interface: X-ray fluorescence study. Phys Rev Lett 1985;54(10):1039. First XSW fluorescence measurements on liquid/gas interface.
[55] Bloch JM, Yun WB, Yang X, Ramanathan M, Montano PA, Capasso C. Adsorption of counterions to a stearate monolayer spread at the water–air interface: a synchrotron X-ray study. Phys Rev Lett 1988;61(26):2941.
[56] • Daillant J, Bosio L, Benattar JJ, Blot C. Interaction of cations with a fatty acid monolayer. A grazing incidence x-ray fluorescence and reflectivity study. Langmuir 1991;7(4):611–4. Excess of counterions near surfactant monolayer at air/water interface as function of lateral monolayer density.
[57] Antipina MN, Dobner B, Konovalov OV, Shapovalov VL, Brezesinski G. Investigation of the protonation state of novel cationic lipids designed for gene transfection. J Phys Chem B 2007;111(49):13845–50.
[58] • Shapovalov VL, Ryskin ME, Konovalov OV, Hermelink A, Brezesinski G. Elemental analysis within the electrical double layer using total reflection X-ray fluorescence technique. J Phys Chem B 2007;111:3927–34. Competitive adsorption of ions to charged surfactant monolayer at air/water interface.
[59] Abuillan W, Schneck E, Körner A, Brandenburg K, Gutsmann T, Gill T, et al. Physical interactions of fish protamine and antisepsis peptide drugs with bacterial membranes revealed by combination of specular x-ray reflectivity and grazing-incidence x-ray fluorescence. Phys Rev E 2013;88(1):012705.
[60] Shapovalov VL, Dittrich M, Konovalov OV, Brezesinski G. Use of total reflection X-ray fluorescence (TRXF) for the quantification of DNA binding to lipid monolayers at the air– water interface. Langmuir 2010;26(18):14766–73.
[61] Zheludeva SI, Novikova NN, Konovalov OV, Kovalchuk MV, Stepina ND, Tereschenko EY. Langmuir monolayers on water surface investigated by X-ray total reflection fluorescence. Mater Sci Eng C 2003;23:567–70.
[62] Körner A, Abuillan W, Deichmann C, Rossetti FF, Köhler A, Konovalov OV, et al. Quantitative determination of lateral concentration and depth profile of histidine-tagged recombinant proteins probed by grazing incidence X-ray fluorescence. J Phys Chem B 2013;117(17):5002–8.
[63] •• Padmanabhan V, Daillant J, Belloni L, Mora S, Alba M, Konovalov OV. Specific ion adsorption and short-range interactions at the air aqueous solution interface. Phys Rev Lett 2007;99:086105. Precise determination of the weak ion depletion at the bare air/water interface.
[64] • Bu W, Mihaylov M, Amoanu D, Lin B, Meron M, Kuzmenko I, et al. X-ray studies of interfacial strontium–extractant complexes in a model solvent extraction system. J Phys Chem B 2014;118(43):12486–500. Quantification of heavy ion amounts immobilized at oil/water interfaces.
[65] Bu W, Yu H, Luo G, Bera MK, Hou B, Schuman AW, et al. Observation of a rare earth Ion-extractant complex arrested at the oil–water interface during solvent extraction. J Phys Chem B 2014;118(36):10662–74.
[66] Krämer M, von Bohlen A, Sternemann C, Paulus M, Hergenröder R. X-ray standing waves: a method for thin layered systems. J Anal At Spectrom 2006;21(11):1136–42.
[67] Zheludeva S, Novikova NN, Stepina N, Yurieva E, Konovalov OV. Molecular organization in protein–lipid film on the water surface studied by x-ray standing wave measurements under total external reflection. Spectrochim Acta B At Spectrosc 2008;63(12):1399–403.
[68] Mughabghab SF. Atlas of neutron resonances: resonance parameters and thermal cross sections. Z = 1–100. Elsevier; 2006.
[69] Aksenov VL, Cser L, Gundorin NA, Nikitenko YuV, Popov YuP. Observation of neutron standing waves at total reflection of polarized neutrons by precision gamma-spectroscopy. Phys B Condens Matter 2000;276–278:809–10.
[70] Aksenov VL, Nikitenko YuV, Radu F, Gledenov YuM, Sedyshev PV. Observation of resonance enhanced neutron standing waves through (n, alpha) reaction. Phys B Condens Matter 2000;276:946–7.
[71] Aksenov VL, Nikitenko YuV, Kozhevnikov SV, Radu F, Kruijs R, Rekveldt MTh. Generation of neutron standing waves at total reflection of polarized neutrons. J Surf Invest 2001;116:1225.
[72] Aksenov VL, Ignatovich VK, Nikitenko YV. Neutron standing waves in layered systems. Crystallogr Rep 2006;51(5):734–53.
[73] Aksenov VL, Nikitenko YV. Neutron interference at grazing incidence reflection. Neutron standing waves in multilayered structures: applications, status, perspectives. Phys B Condens Matter 2001;297(1):101–12.
[74] unpublished data.
[75] Bauer C, Bauduin P, Dufrêche JF, Zemb T, Diat O. Liquid/liquid metal extraction: phase diagram topology resulting from molecular interactions between extractant, ion, oil and water. Eur Phys J Spec Top 2012;213(1):225–41.